

Warm Dark Matter versus Bumpy Power Spectra

Brett Little¹, Alexander Knebe¹, Ranty R. Islam²

¹*Centre for Astrophysics & Supercomputing, Swinburne University, P.O. Box 218, Mail # 31, Hawthorn, Victoria, 3122, Australia*

²*Astrophysics, Keble Road, Oxford, OX1 3RH, UK*

Received ...; accepted ...

ABSTRACT

In this paper we are exploring the differences between a Warm Dark Matter model and a CDM model where the power on a certain scale is reduced by introducing a narrow negative feature (“dip”). This dip is placed in a way so as to mimic the loss of power in the WDM model: both models have the same integrated power out to the scale where the power of the Dip model rises to the level of the unperturbed CDM spectrum again.

Using N -body simulations we show that some of the large-scale clustering patterns of this new model follow more closely the usual CDM scenario while simultaneously suppressing small scale structures (within galactic halos) even more efficiently than WDM. The analysis in the paper shows that the new Dip model appears to be a viable alternative to WDM but it is based on different physics. Where WDM requires the introduction of a new particle species the Dip model is based on a non-standard inflationary period. If we are looking for an alternative to the currently challenged standard Λ CDM structure formation scenario, neither the Λ WDM nor the new Dip model can be ruled out based on the analysis presented in this paper. They both make very similar predictions and the degeneracy between them can only be broken with observations yet to come.

Key words: cosmology – numerical simulations

1 INTRODUCTION

The so-called Cold Dark Matter crisis has led to a vast number of publications trying to solve the problems which seem to be associated with an excess of power on small scales. One possibility to reduce this power is to introduce Warm Dark Matter (i.e. Knebe et al. 2002; Bode, Ostriker & Turok 2001; Avila-Reese et al. 2001; Colin et al. 2000). But another way to decrease power on a certain scale is to introduce a negative feature (“dip”) into an otherwise unperturbed CDM power spectrum.

Several mechanisms have been proposed that could generate such features in the primordial spectrum during the epoch of inflation. Among these are models with Broken Scale Invariance (BSI) (Lesgourgues, Polarski & Starobinsky 1998), and particularly BSI due to phase transitions during inflation (Barriga et al. 2000). Other inflationary models include resonant production of particles (Chung et al. 1999) and non-vacuum initial states as the quantum mechanical origin for inflationary perturbations (Martin, Riazuelo & Sakellariadou 2000). Broad features can also be introduced into the power spectrum by including a running spectral index in slow-roll inflationary models (e.g. Hannestad, Hansen & Villante 2000). However, the parameter range for such broad features is rela-

tively tightly constrained by observational data from the BOOMERanG (de Bernardis et al. 2000) and MAXIMA experiments (Balbi et al. 2000), and some of the features tend to be too broad to be able to yield the scale-dependent effects on the power spectrum we consider here. After inflation, other effects such as pressure-induced oscillations* in the matter radiation fluid before decoupling also leave an imprint in the overall matter transfer function towards small scales mainly in the form of successive crests and troughs (Eisenstein & Hu 1998). These features will therefore also be part of the cosmological matter power spectrum after matter-radiation equality. Only for extraordinarily large baryon fractions will these features be significant enough to affect the subsequent formation of small and medium scale structures.

Most of the above mechanisms appear capable of producing localized features on any given scale, but to date only large scales have been tested quantitatively. The non-vacuum initial state model by Martin, Riazuelo & Sakellariadou (2000), for instance, can lead to a primordial $P(k)$ with a sharply localized peak, where the location k_0 of that

* This is also recorded in the oscillatory nature of the spectrum of the cosmic microwave background fluctuations.

peak is determined by a characteristic built-in scale of their model. On the other hand, a negative feature is possible BSI scenarios which lead to oscillations beyond a certain scale in $P(k)$ (Lesgourgues, Polarski & Starobinsky 1998). As N -body simulations are limited in the k -range modeled, one might only be able to trace the first dip of those oscillations due to a privileged energy within the inflaton potential that determines the scale k_0 .

Our objective now is to examine the effect of a negative feature in the primordial power spectrum at very small scales that directly affects the formation and evolution of (sub-)galactic halos. In particular we have chosen a negative Gaussian feature on a scale ($k \simeq 1.8h\text{Mpc}^{-1}$). We have not tied our analysis to any of the above models, but we have adopted a more generic approach modeling the dip as a Gaussian in log-space (see below). This differs from earlier studies of 'bumpy power spectra' (e.g. Lewin & Albrecht, 2001). Such a modification is more similar to the idea of Warm Dark Matter, but the difference lies in the rise of power towards even smaller scales. Where WDM cuts off all power exponentially below a certain threshold, we introduce here a model that has a rather narrow dip in $P(k)$ and the detailed shape for the loss of power is completely different, respectively. We have shown in an earlier paper (Knebe, Islam & Silk 2001) that such localized features in the matter power spectrum can obscure the interpretation of the evolution of cluster abundance as an indicator of the cosmological density parameter. In this paper we are now going to show that a similar feature (but on smaller scales) can lead to comparable results as for instance a Warm Dark Matter model. This Dip model can hence be understood as a plausible alternative to WDM without making assumptions about the nature of dark matter and only further studies (and observations) might break the degeneracy between those models found in this analysis.

The structure of this paper closely follows that of the WDM investigation by Knebe et al. (2002). We chose to study the same properties, but this time focusing on the comparison between the ΛWDM and the new Dip model. We first start with a brief description of the newly introduced Dip model in Section 2, then move on to the simulations themselves in Section 3. In Section 4 we analyze the output from our numerical simulations highlighting the differences in the ΛWDM and the Dip model. We finally summarize our results and conclude in Section 5.

2 THE DIP-MODEL

The ΛWDM and the fiducial ΛCDM model used in this paper are the same as those used in Knebe et al. (2002) with the cosmological parameters $\Omega_0 = 1/3$, $\lambda_0 = 2/3$, $\sigma_8 = 0.88$, $h = 2/3$, and $m_{\text{WDM}} = 0.5\text{keV}$ for ΛWDM .

For the Dip model we are using the same prescription to introduce a Gaussian feature into an otherwise unperturbed CDM power spectrum as outlined in Knebe, Islam & Silk (2001) and hence the modified power spectrum follows the equation:

$$P_{\text{mod}}(k) = P(k) \cdot \left[1 - A \exp \left\{ -0.4 \left(\frac{\log k - \log k_0}{\sigma_{\text{mod}}} \right)^2 \right\} \right] \quad (1)$$

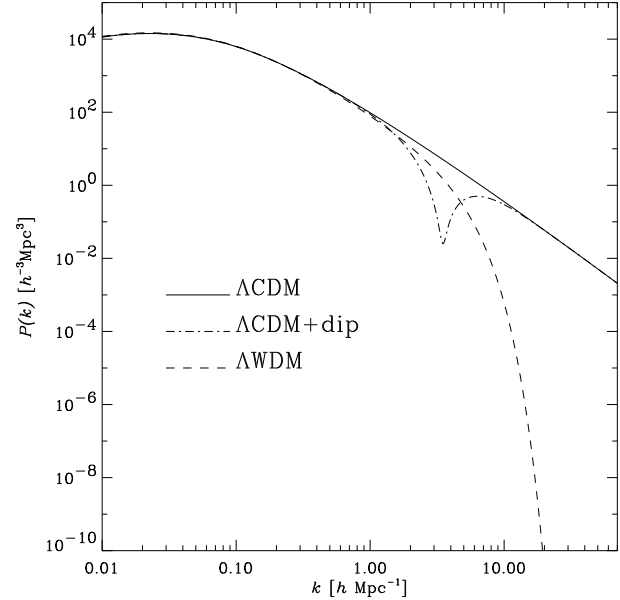


Figure 1. CDM input spectra at redshift $z = 0$.

Table 1. Specifications of the artificial modification to the ΛCDM power spectrum. The mass scale $M = \rho_{\text{crit}} \Omega \cdot \frac{4\pi}{3} (2\pi/k_0)^3$ corresponding to the value of k_0 is given in the last column.

label	$2\pi/k_0$	A	σ_{mod}	mass scale
Dip Model	$1.8h^{-1} \text{ Mpc}$	-0.995	0.5	$2 \cdot 10^{12} M_{\odot}/h$

where $P(k)$ is the unmodified spectrum and the parameters A , σ_{mod} , and k_0 of the dip are given in Table 1.

The power taken away from the standard ΛCDM model via the dip agrees with the lack of power in the ΛWDM model to the extent that the integral

$$\sigma^2 = \frac{1}{2\pi^2} \int_0^{k=16h\text{Mpc}^{-1}} P(k) k^2 dk \quad (2)$$

is identical for the ΛWDM and Dip model ($k = 16h\text{Mpc}^{-1}$ is the point for which the dip meets the unperturbed ΛCDM power spectrum again). The power in the Dip model only drops in a narrow interval around k_0 with the width of that interval controlled by the parameter σ_{mod} . A visualization of the three power spectra used in this study is given in Fig. 1.

Even though the power that has been taken away from the standard ΛCDM model is similar, both models (ΛWDM and Dip) are based on different physics. WDM is realized by postulating a finite mass for the dark matter particles in the range of $m_{\text{WDM}} = 0.5 - 2\text{keV}$ (0.5keV in our case), whereas the Dip model assumes that the CDM picture is still valid but based on a primordial power spectrum that is the result of some non-standard inflationary period as outlined in the Introduction.

3 THE N -BODY SIMULATIONS

The simulations of the ΛWDM and the ΛCDM model were carried out using the Multiple-Mass ART code (Kravtsov,

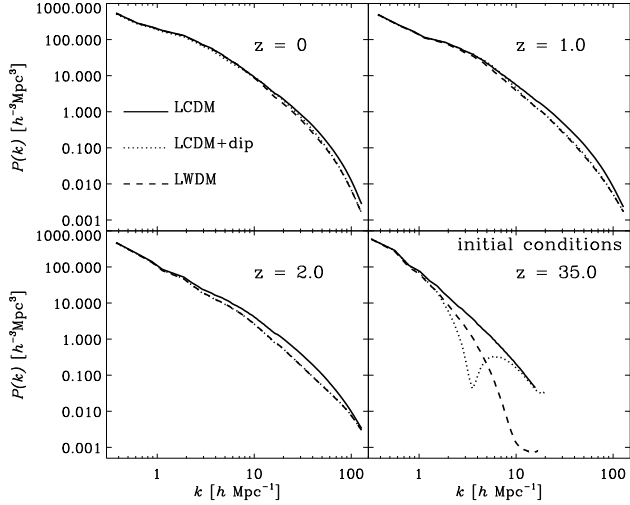


Figure 2. Power spectrum evolution.

Klypin & Khokhlov 1997) and the details for these runs can be found in Knebe et al. (2002). The new Dip model was set up using the same multiple-mass technique but evolved with the publicly available Adaptive Mesh Refinement code **MLAPM** (Knebe, Green & Binney 2001). The number of particles in use for all three runs was 128^3 in a box of comoving side length $25h^{-1}$ Mpc.

As both codes (**ART** and **MLAPM**) are adaptive mesh refinement codes designed in a very similar fashion, the technical details (i.e. refinement criterion, number of integration steps, etc.) are identical to the ones already outlined in Knebe et al. (2002), and hence we obtained the same force resolution of $3h^{-1}$ kpc in the new Dip model. A quantitative comparison of these two codes can be found in Knebe, Green & Binney (2001) where it is shown that both produce (nearly) identical results when being run with the same parameter setup. As the realizations of the initial density field were identical too for all simulations, we are able to undertake a one-to-one comparison of the two most massive haloes in all three models.

The halos in each individual model were identified using both the friends-of-friends algorithm (FOF, Davis et al. 1985) and the Bound-Density-Maxima (BDM, Klypin & Holtzman 1997) method.

4 ANALYSIS

4.1 Power Spectra

Fig. 2 shows $P(k)$ as derived from our initial particle distribution at redshift $z = 35$ along with the non-linear evolution at redshifts $z = 2$, $z = 1$ and $z = 0$.

The Dip is well resolved by our initial conditions and lies inside the k -range defined by the box size $B=25h^{-1}$ Mpc ($k_{\min} = 2\pi/B$) and the particle Nyquist frequency as determined by the total number of particles $N=128^3$ ($k_{\max} = \pi/\Delta x$ with $\Delta x = B^3/N$).

We can also clearly see that the transfer of power from large to small scales washes out the features initially present in the power spectrum at our starting redshift. The major

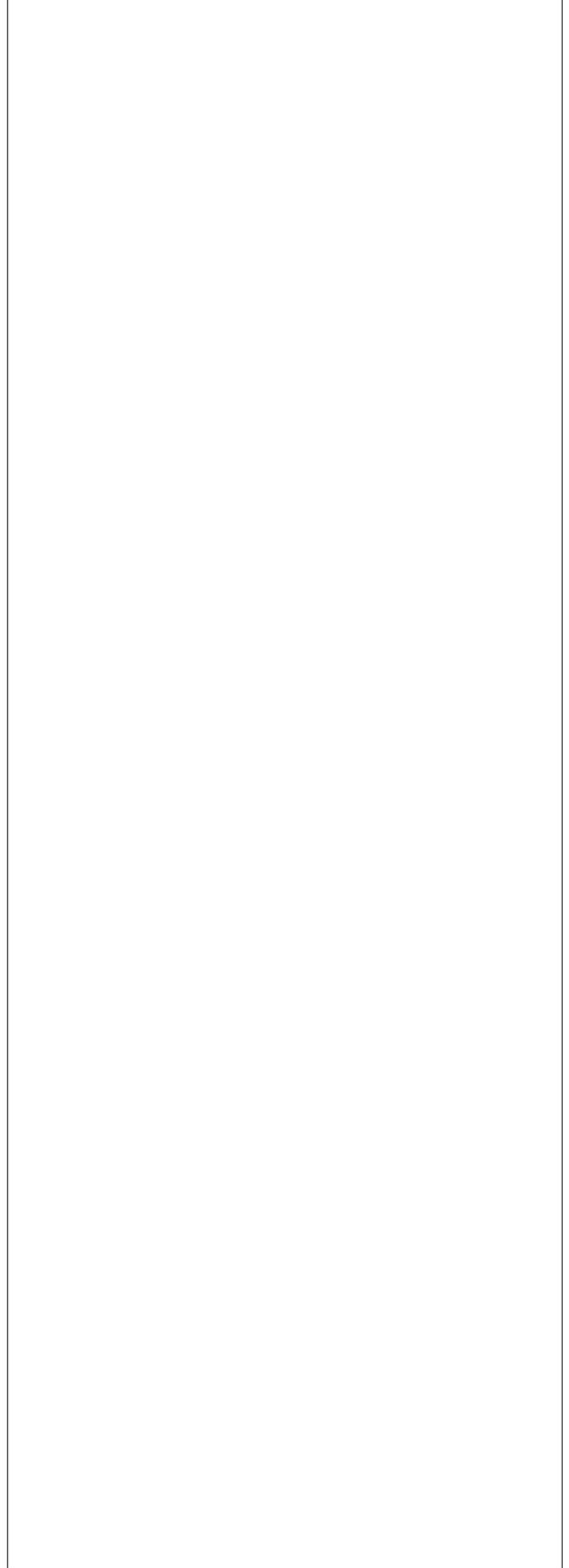


Figure 3. Grey-scaled density field of a $10 \times 10 h^{-1}$ Mpc slice through the simulation at $z = 0$.

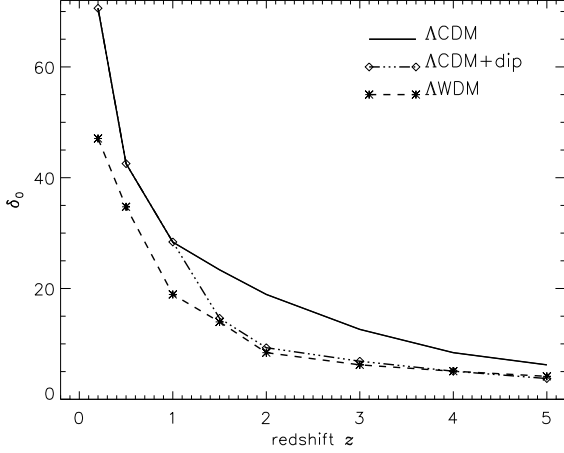


Figure 4. Threshold density contrast δ_0 (defined via $\dot{\rho}(\delta_0) = 0$) as a function of redshift for all three models.

difference between the WDM and the Dip model in the simulations is that the loss of power is far steeper in the latter but also rises again to the level of the unperturbed Λ CDM spectrum. In the WDM model the power decreases more gradually and monotonically. We will see that this has an effect on the formation of low- and high-mass halos as well as the amount of substructure to be found in galactic halos. However, the general predictions of both models remain similar.

Unfortunately we are unable to study the formation process of objects smaller than $10^{10} h^{-1} M_\odot$ because of the limits imposed by the total number of particles used. Our mass resolution is “only” $m_p \sim 7 \cdot 10^8 h^{-1} M_\odot$ and hence we cannot initially resolve the regime $k > 16 h \text{Mpc}^{-1}$ where the amplitude of the power spectrum in the Dip and the Λ CDM models join up again.

4.2 Dark Matter Density Field

We continue our analysis by inspecting the large-scale structure density field in all three runs. In Fig. 3 we show a slice through the particle distribution for all three models with the particles grey-scaled according to the local overdensity (emphasizing on low density regions).

We can clearly see the “lumpiness” of Λ CDM against Λ WDM and the Dip model, respectively. But when comparing Λ WDM with the Dip model we notice that the filamentary structure of the Universe appears to be slightly more grainy/evolved in the latter. As pointed out elsewhere (Knebe et al. 2002; Bode, Ostriker & Turok 2000) small size objects tend to form in WDM preferably via filament fragmentation as well as at later times. This phenomenon might not be the case for the Dip model anymore; we expect to find the filaments to be more clumpy initially because the power on very small scales rises again to the level of the “normal” CDM spectrum. And this can be clearly seen in Fig. 3; the low density dark matter particles appear to be more clustered (within the filaments) as opposed to a more smooth distribution in WDM. The similarity between CDM and the Dip model for low-density regions can be even more

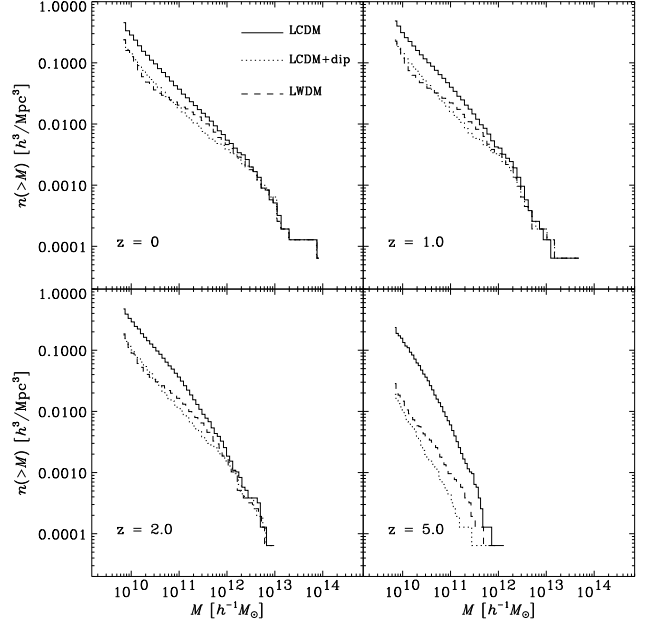


Figure 5. Evolution of mass function.

emphasized when calculating $\dot{\rho}$, the flow of matter. To this extent we used the continuity equation

$$\dot{\rho} = \partial\rho/\partial t = -\nabla \cdot (\rho\vec{v}), \quad (3)$$

where the rhs was calculated on a 300^3 grid covering the whole computational volume. The function $\dot{\rho}(\delta)$ with $\delta = \rho/\bar{\rho} - 1$ has one root in the regime $\delta < 200$ because matter flows out of low density into high density regions. This defines a ‘threshold density’ δ_0 via

$$\dot{\rho}(\delta_0) = 0. \quad (4)$$

The redshift evolution of this δ_0 is presented in Fig. 4 for all three models. We note that δ_0 is at all times larger in Λ CDM than in Λ WDM. This can be explained by a faster flow of material out of the voids and into the filaments; the threshold density δ_0 where the inflow of matter equals the outflow is shifted towards higher density regions. But the Dip model shows a break at redshift around $z = 1.5$. At later times it agrees with Λ CDM whereas it matches the Λ WDM model at higher redshifts. However, this behavior is difficult to test observationally as we investigated the flow of low density material. An analysis of the two-point correlation function of objects in the mass range $10^{10} h^{-1} M_\odot < M < 10^{11} h^{-1} M_\odot$ though showed a higher (and matching) clustering amplitude for Λ WDM and the Dip model when compared to Λ CDM.

4.3 Mass Function of Halos

A quantitative difference between the Dip and the Λ WDM model with respect to galactic halos becomes apparent when calculating the (cumulative) mass function $n(> M)$ as a function of redshift z . Fig. 5 shows $n(> M)$ for all three models at redshifts $z = 5, 2, 1,$ and 0 . In addition to the fact that the Dip and the Λ WDM model show a similar behavior we also note that, first, at higher redshifts there are fewer

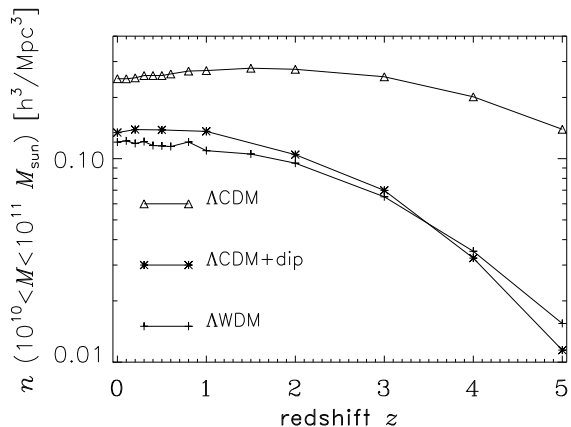


Figure 6. Evolution of halo abundance for particle groups with mass M in the range $[10^{10}h^{-1}M_{\odot}, 10^{11}h^{-1}M_{\odot}]$.

high mass objects for the Dip model than for Λ WDM and second, the curve for the Dip model for $M < 5 \times 10^{11}h^{-1}M_{\odot}$ runs parallel at all times (but lower in amplitude) to the fiducial Λ CDM model.

The former can be explained again by the fact that the drop of power compared to WDM is sharper in the Dip model; the "excess-lack" of power is on scales that roughly agree with objects of the order $\sim 10^{11}h^{-1}M_{\odot}$, which coincides with the high-mass end of mass function at redshift $z = 5$. However, during the course of the simulation the high mass end of the (Dip)-mass function converges to the level of the Λ CDM model.

The latter can be ascribed to the rise of power in the Dip model which seems to counter act the top-down fragmentation of the filaments found in the WDM structure formation scenario (i.e. Knebe et al. 2002; Bode, Ostriker & Turok 2001) in such a way that they tend to be more grainy initially (as already seen in Fig. 3). But those small particle groups do not make it into larger objects as we lack power on the "connecting" scales; they stay isolated within the filaments.

In Fig. 6 we highlight the number density evolution of objects in the mass range $10^{10}h^{-1}M_{\odot} < M < 10^{11}h^{-1}M_{\odot}$ by plotting the abundance evolution for particle groups within that range out to redshift $z = 5$. Again, the behavior for WDM and the Dip model are very similar, but we see the trend for a steeper and faster evolution in the latter.

4.4 Individual Halos

The remaining analysis will focus on the two most massive halos found in all three runs. To this extent we start with showing the density fields of those two objects. Fig. 7 confirms again that the damping of small scale power in the primordial power spectrum leads to a suppression of substructure in galactic halos. But we can also see that this suppression is far more pronounced in the Dip model than in the WDM structure formation scenario. We attribute this again to the steeper cut-off in the primordial power spectrum.

To quantify these finding we calculated the cumulative circular velocity distribution of satellites within halo #1 and

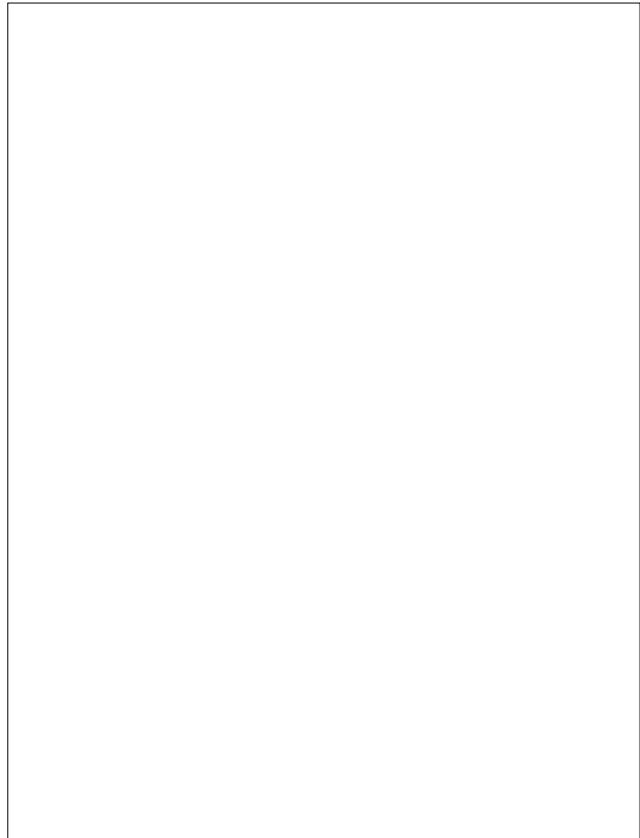


Figure 7. Gray-scaled density field of the two most massive galactic halos identified at $z=0$. The left panel shows halo #1 of mass $9.3 \cdot 10^{13}h^{-1}M_{\odot}$ (about 135000 particles) and the right panel shows halo #2 weighing $8.2 \cdot 10^{13}h^{-1}M_{\odot}$ (ca. 120000 particles). The upper most panel is for the Λ CDM model, the middle panel shows the Λ WDM run, and the lower panel is the new Dip model.

Table 2. Number of satellite galaxies orbiting in halo #1 and halo #2.

model	halo #1		halo #2	
	$z = 0$	$z = 1$	$z = 0$	$z = 1$
Λ CDM	42	48	29	12
Λ WDM	29	28	29	11
Λ CDM+dip	30	19	29	11

halo #2. The result can be found in Fig. 8 which is accompanied by Table 2 where we give the total numbers of satellites found in each halo at redshifts $z = 0$ and $z = 1$, respectively.

There is clear evidence that the Dip model produces even fewer satellites than WDM. Even though there are roughly the same number of satellites at redshift $z = 1$ in all three models, their number only marginally increases in the Dip model (especially for halo #2). We previously interpreted the suppression of substructure in WDM by balancing the accretion and destruction rate of satellites in the halo (Knebe et al. 2002); as such, the even higher destruction rate in the Dip model can best be explained by the presence even more loosely bound satellites. This again can be ascribed to the faster drop-off in power and can therefore be controlled by the amplitude A and the width σ_{mod} of the

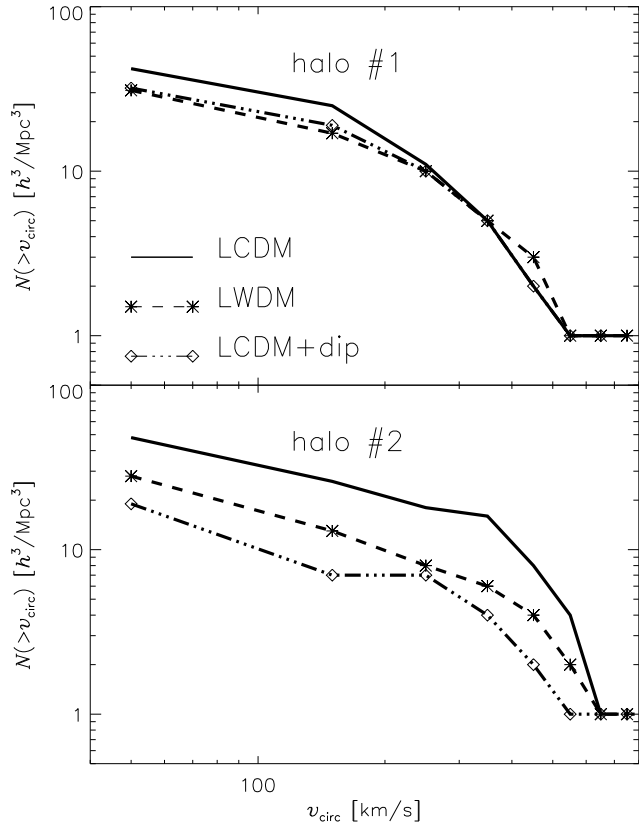


Figure 8. Cumulative circular velocity distribution of satellites orbiting in halo #1 and halo #2 for $z = 0$.

Dip. However, tuning the Dip parameters to bring the number of satellites into agreement with the WDM model will automatically have an effect on, for instance, the mass function as given in Fig. 5. The lower the amplitude the closer it should get to the unperturbed Λ CDM model. Hence the Dip model provides a way of suppressing substructure but otherwise reproducing the standard CDM structure formation scenario. The even milder increase in number of satellites for halo #2 in the Dip model (cf. Table 2 and Fig. 8) is readily explained by the fact that that particular halo underwent a major merger near redshift $z = 0.2$. The tidal effects of such a merger tend to destroy the loosely bound satellites in that model more successfully and hence we are left with even fewer than in the Λ WDM model.

5 SUMMARY AND DISCUSSION

We investigated the differences of two models that both suppress small scale fluctuations in the primordial power spectrum, namely a warm dark matter and the newly introduced Dip model. While it may be argued that the Λ WDM model is better constrained in terms of the allowed masses and thus free streaming length of the potential particle candidates, the Dip model considered here makes no assumption about the nature of the dark matter component. This happens at the expense of introducing two additional parameters (the amplitude A and width σ_{mod} of the dip), although these are determined entirely by inflationary physics and thus before

decoupling (on the basis of the models considered in the Introduction). Using both the Λ WDM and the Dip model as the input to N -body simulations we showed that their predictions are fairly similar with a few notable differences.

The dip in our model was chosen to mimic the loss of power in a WDM Universe in a sense that the integrated power (out to the point where the dip reaches the unperturbed Λ CDM level again) in both models is identical. Therefore all differences to be found in the structure formation process are due to the way in which power on small scales is suppressed and the detailed shape of the power spectrum, respectively. The analysis presented in this paper showed that the way the loss of power is realized is only of minor importance for objects within the mass range under investigation. However, there are some quantitative differences, mainly in the shape of the cumulative mass function at the low mass end and the flow of low density material.

For the Dip model the low density material appears to be more in line with that expected for CDM (cf. Fig. 4). This agreement may reflect the rise in power to that of CDM on very small scales. To quantify this effect more accurately, the resolution has to be improved significantly, but on theoretical grounds this behavior is expected. In filaments the ‘background overdensity’ contributed by large wave length modes tends to be lower than in highly clustered regions and consequently the onset of non-linear evolution of the smallest scales will occur later than in cluster environments. In this case traces of the rise in the linear power spectrum at very small scales may be more likely to be observable here than in the clustered regions at the present day. Observations of structures residing in filaments could therefore potentially help to constrain the power spectrum on these very small scales.

Despite the similarities in filamentary structure of the Dip and CDM model compared to the WDM model, the suppression of low-mass halos is even more pronounced. This even stronger suppression of substructure (in galactic halos) can easily be explained by the amplitude of the dip and an adequate choice for A will definitely eliminate the deviation from the WDM model. But in that case one will also automatically alter the formation times and sites for low mass halos in general bringing it more into agreement with CDM. The Dip model hence provides a way of fine tuning the number of satellites without deviating too far from the standard CDM paradigm (cf. Fig. 4 and Fig. 5) otherwise.

The other difference between WDM and the Dip model is the shape of the cumulative mass function and the evolution and formation times of halos. Here we showed that even though small mass objects (as well as high mass objects) are suppressed, the shape of $n(>M)$ follows more closely that of the Λ CDM model; the power law behavior at the low mass end is preserved. We interpreted this result with respect to the rise of power in the Dip model which counteracts the top-down fragmentation of filaments. The filaments are more grainy/evolved initially due to the relative excess of power on very small scales compared to the WDM model (cf. Fig. 3). Moreover, the lack of high-mass halos at high redshift in the Dip model might allow us to observationally distinguish between WDM and the Dip model.

The resolution of our simulations did not allow for a more detailed comparison of the models on very small (mass) scales where the Dip model has the same power as the

Λ CDM model again. This we postpone to a future investigation.

To conclude, we remark that the Dip model has proven to be a viable alternative to the WDM structure formation scenario and only future observations as well as better resolved numerical simulations will be able to disentangle the degeneracy between those two models. The only way of breaking this degeneracy might lie within the filamentary structures of the Universe and the low-mass end of the cumulative mass function. Our results suggested a simple power-law behavior for these scales (similar to the Λ CDM model) whereas the shape of the mass function in the WDM case is more complicated. But to strengthen these findings we clearly need more detailed and much better resolved simulations in the future.

ACKNOWLEDGMENTS

We benefitted from valuable discussions with Brad Gibson. The simulations presented in this paper were carried out on the Beowulf cluster at the Centre for Astrophysics & Supercomputing, Swinburne University and the Oxford Supercomputer Centre. We are grateful to Anatoly Klypin and Andrey Kravtsov for kindly providing a copy of the ART code that was used for running the Λ CDM and Λ WDM simulation, respectively. We acknowledge the support of the Swinburne University Research Development Grants Scheme.

REFERENCES

- Avila-Reese V., Colin P., Valenzuela O., D’Onghia E., Firmani C., *ApJ* **559**, 516 (2001)
- Balbi A., et al., [astro-ph/0005124](#)
- Barriga J., Gaztañaga E., Santos M.G, Sarkar S. *MNRAS* **324**, 977 (2001)
- de Bernardis P., et al., *Nature* **404**, 955 (2000)
- Bode P., Ostriker J.P., Turok N., *ApJ* **556**, 93 (2001)
- Chung D.J.H., Kolb E.W., Riotto A., Tkachev I.I., [hep-ph/9910437](#) (1999)
- Colin P., Avila-Reese V., Valenzuela O., *ApJ* **542**, 622 (2000)
- Davis M., Efstathiou G., Frenk C.S., White S.D.M., *ApJ* **292**, 371 (1985)
- Eisenstein D., Hu W. *ApJ* **496**, 605 (1998)
- Hannestad S., Hansen S.H., Villante F.L., *Astropart.Phys.* **16**, 137 (2001)
- Klypin A.A., Holtzman J., [astro-ph/9712217](#)
- Knebe A., Green A., Binney J., *MNRAS* **325**, 845 (2001)
- Knebe A., Islam R.R., Silk J., *MNRAS* **326**, 109 (2001)
- Knebe A., Devriendt J., Mahmood A., Silk J., *MNRAS* **329**, 813 (2001)
- Kravtsov A.V., Klypin A.A., Khokhlov A.M., *ApJ* **111**, 73 (1997)
- Lesgourgues J., Polarski D., Starobinsky A.A., *MNRAS* **297**, 769L (1998)
- Lewin A., Albrecht A., *Phys. Rev.* **D64**, 023514 (2001)
- Martin J., Riazuelo A., Sakellariadou M., *Phys. Rev.* **D61**, 083518 (2000)
- Press W.H., Schechter P., *ApJ* **187**, 425 (1974)

This figure "fig03.jpg" is available in "jpg" format from:

<http://arxiv.org/ps/astro-ph/0205420v2>

This figure "fig07.jpg" is available in "jpg" format from:

<http://arxiv.org/ps/astro-ph/0205420v2>